Androctonin, a hydrophilic disulphide-bridged non-haemolytic anti-microbial peptide: a plausible mode of action

Charles HETRU*[1], Lucienne LETELLIER†, Ziv OREN‡, Jules A. HOFFMANN* and Yechiel SHAI‡

*UPR 9022, CNRS, 'Réponse Immunitaire et Développement chez les Insectes', Institut de Biologie Moléculaire et Cellulaire, 15, rue René Descartes, 67084 Strasbourg Cedex, France, †UMR 8619 CNRS, Laboratoire des Biomembranes, Université Paris-Sud, Bâtiment 433, 91405 Orsay Cedex, France, and ‡Department of Biological Chemistry, Weizmann Institute of Science, Rehovot 76100, Israel

Androctonin is a 25-residue non-haemolytic anti-microbial peptide isolated from the scorpion *Androctonus australis* and contains two disulphide bridges. Androctonin is different from known native anti-microbial peptides, being a relatively hydrophilic and non-amphipathic molecule. This raises the possibility that the target of androctonin might not be the bacterial membrane, shown to be a target for most amphipathic lytic peptides. To shed light on its mode of action on bacteria and its non-haemolytic activity, we synthesized androctonin, its fluorescent derivatives and its all-D-amino acid enantiomer. The enantiomer preserved high activity, suggesting a lipid–peptide interaction between androctonin and bacterial membranes. In Gram-positive and (at higher concentrations) Gram-negative bacteria, androctonin induced an immediate perturbation of the permeability properties of the cytoplasmic membrane of the bacterial energetic state, concomitant with perturbation of the morphology of the cell envelope as revealed by electron microscopy. Androctonin binds only to negatively charged lipid vesicles and induces the leakage of markers at high concentrations and with a slow kinetics, in contrast with amphipathic α-helical anti-microbial peptides that bind and permeate negatively charged vesicles, and to a smaller extent also zwitterionic ones. This might explain the selective lytic activity of androctonin towards bacteria but not red blood cells. Polarized attenuated total reflection–Fourier transform infrared spectroscopy revealed that androctonin adopts a β-sheet structure in membranes and did not affect the lipid acyl chain order, which supports a detergent-like effect. The small size of androctonin, its hydrophilic character and its physicochemical properties are favourable features for its potential application as a replacement for commercially available antibiotics to which bacteria have developed resistance.

Key words: fluorescent spectroscopy, lipid–peptide interaction, scorpion.

INTRODUCTION

Anti-microbial peptides in living organisms serve as a defence system in addition to, or complementary to, the highly specific cell-mediated immune response. This secondary, chemical, immune system provides the organisms with a group of small peptides that are promptly synthesized on induction, and act against the invasion of occasional or obligate pathogens (reviewed in [1–4]). Anti-microbial peptides were initially discovered in invertebrates [5] and subsequently also in vertebrates [6,7], including humans [8]. Interestingly, the phylum of the arthropods has so far yielded the largest number of anti-microbial peptides, with the greatest diversity [9].

Anti-microbial peptides can be divided into four major groups.

(1) Linear, mostly helical peptides, without cysteine residues. This intensely investigated group includes short linear polypeptides (at most 40 residues) devoid of disulphide bridges, e.g. cecropins, isolated from the moth *Hyalophora cecropia* [5], and magainins [7] and dermaseptins [10] from frog skins. These peptides vary considerably in chain length, hydrophobicity and overall distribution of charges, but share a common α-helical structure when associated with phospholipid membranes [11].

(2) Linear peptides without cysteine residues and with a high proportion of proline and arginine residues [12].

(3) Peptides containing disulphide bonds involving an α-helix and a twisted β-sheet [13] or forming only β-sheet structures with anti-parallel chains [1].

(4) Large (10–30 kDa) glycine-rich polypeptides [9].

In comparison with the wealth of studies on the mode of action of amphipathic α-helical peptides [14–16], the cysteine-containing peptides have been poorly explored. Members of this group include α-defensins [17], β-defensins [18], protegrins [19] and tachyplesins [20].

A novel cysteine-rich anti-microbial peptide has been isolated and characterized from the blood of the scorpion *Androctonus australis* [21]. This peptide is composed of 25 residues and contains two disulphide bridges (RSVCRQIKICRRRGGCYYKCTNRPY, cysteine array: Cys^4–Cys^{20} and Cys^{10}–Cys^{16}). Androctonin inhibits the growth of both Gram-positive and Gram-negative bacteria and has in addition a large spectrum of activity against filamentous fungi. However, no haemolytic activity is observed at concentrations up to 150 μM, which corresponds to 50-fold the mean minimal inhibitory concentration (MIC) [21]. Androctonin represents a special type of anti-microbial peptide because it is a relatively hydrophilic, non-amphipathic molecule (approx. 30% hydrophobic amino acids). This contrasts with the amphipathic α-helical anti-microbial peptides, which are composed of more than 50% hydrophobic amino acids. This observation raises the possibility that the target of androctonin is not the lipid component of the bacterial membrane, an established target of many linear amphipathic α-helical anti-microbial peptides.

To investigate the mode of action of androctonin we have used a synthetic molecule corresponding to the sequence of the native

Abbreviations used: ATR–FTIR, attenuated total reflection–Fourier transform infrared; Fmoc, fluoren-9-ylmethoxycarbonyl; MIC, minimal inhibitory concentration; NBD, 4-fluoro-7-nitrobenz-2-oxa-1,3-diazole; PtdCho, egg phosphatidylcholine; PtdEtn, phosphatidylethanolamine; PtdGro, egg phosphatidylglycerol; PtdSer, bovine spinal cord phosphatidylserine; Rho, carboxytetramethylrhodamine succinimidyl ester; SUV, small unilamellar vesicles.

[1] To whom correspondence should be addressed (e-mail hetru@ibmc.u-strasbg.fr).

peptide with or without fluorescence probes bound to the N-terminus. Our results show that androctonin disrupts the permeability barrier of the cytoplasmic membrane of *Micrococcus luteus* and *Escherichia coli* and binds preferentially to negatively charged vesicles, as with linear α-helical anti-microbial peptides. However, in contrast with the α-helical peptides, the ability of androctonin to cause calcein leakage from vesicles depends on the charge of the phospholipid headgroup. The results also show that the activity of all-D-amino acid androctonin is similar to that of the all-L-amino acid molecule, which further suggests that it binds non-specifically to the bacterial membrane rather than to a specific receptor.

MATERIALS AND METHODS

Materials

Egg phosphatidylcholine (PtdCho) and bovine spinal cord phosphatidylserine (PtdSer) (sodium salt, grade I), were purchased from Lipid Products (South Nutfield, Surrey, U.K.). Egg phosphatidylglycerol (PtdGro) and phosphatidylethanolamine (PtdEtn) (type V, from *Escherichia coli*) were purchased from Sigma; 5- (and 6)-tetramethylrhodamine succinimidyl ester and 4-fluoro-7-nitrobenz-2-oxa-1,3-diazole ('NBD-F') were obtained from Molecular Probes. Calcein was purchased from Hach Chemical Co. (Loveland, CO, U.S.A.). All other reagents were of analytical grade.

Peptide synthesis and fluorescent labelling

Fluoren-9-ylmethoxycarbonyl (Fmoc) amino acid derivatives were purchased from Neosystem (Strasbourg, France). Assembly of the protected peptide chain was performed on a 25 μmol scale with a home-made multichannel peptide synthesizer with classic Fmoc methodology, as described [22]. The resin-bound peptide, with its amino acid side chains fully protected, was treated with piperidine to remove the Fmoc protecting group from its N-terminal amino group, while keeping all the other reactive amine groups of the attached peptide still protected. Resin-bound peptide (30 mg; 10 μmol) was then reacted with the desired fluorescent probe (30 μmol) in dry dimethylformamide for 48 h, washed thoroughly with methylene chloride and then cleaved from the resin by trifluoroacetic acid, extracted and finally precipitated with ether. The pellet containing the reduced peptide was taken up in 0.1 M ammonium acetate buffer, pH 8.5, at a concentration of 35 mg/l and was allowed to refold by oxidation in air for 24 h at room temperature under stirring. The labelled peptide was purified by HPLC and the structure of the synthetic refolded peptide was confirmed by electrospray MS analysis and by the use of endoproteinase Lys-C, the disulphide array was shown to be identical with that of the native peptide (i.e. Cys^{4}–Cys^{20} and Cys^{10}–Cys^{16}) (see [21]).

Bacterial strains and cell growth

The peptides were tested for their anti-microbial activity against a representative set of bacteria, including two Gram-positive species: *M. luteus* A270 (Pasteur Institute Collection) and *Aerococcus viridans* (obtained from H. Monteil, Institute of Bacteriology, University of Strasbourg, Strasbourg, France), and two Gram-negative bacteria, *Escherichia coli* D21 and D31 (obtained from H. G. Boman, Institute of Microbiology, University of Stockholm, Stockholm, Sweden). Bacteria were grown aerobically at 37 °C in Luria–Bertani medium [0.5% yeast extract/1% (w/v) Bacto-Tryptone/1% (w/v) NaCl], pH 7. For K^+ efflux experiments, cells were harvested at a D_{600} of 0.5, then washed and resuspended in 10 mM Hepes buffer containing a variable concentration of NaCl, pH 7.8, at a D_{600} of 50. They were kept at room temperature (to prevent the loss of cytoplasmic K^+) and used within 3 h.

Anti-bacterial assays and determination of the MIC

The anti-bacterial activity of the peptides was determined with a liquid-growth inhibition assay as described in [23]. In brief, 10 μl aliquots from 2-fold serial concentrations were incubated in microtitre plates with 100 μl of a mid-exponential-phase culture of bacteria at a starting D_{600} of 0.001. The bacteria were left to grow for 24 h at 25 °C; growth was evaluated by D_{600} with a microplate reader. The MIC was expressed by the method of Casteels et al. [24] as an interval ($a-b$), where a is the highest concentration tested at which bacteria are growing and b is the lowest concentration that inhibits the bacterial growth.

K^+ efflux measurements

The K^+ efflux from Gram-positive (*M. luteus* A270) and Gram-negative (*E. coli* D21) bacteria was monitored by measuring the extracellular K^+ concentration with a K^+/valinomycin-selective electrode (Radiometer) at 37 °C, as described previously [25]. In most cases *M. luteus* and *E. coli* cells were resuspended in assay medium containing 10 mM Hepes, pH 7.4, 10 or 150 mM NaCl and 0.5 mM KCl. *M. luteus* (3 ml, 0.31 mg dry weight of cells/ml [25]) and *E. coli* (3 ml, 0.5 mg dry weight of cells/ml [26]) were energized by the addition of 0.2% glucose. Internal K^+ (K^+_{in}) content was expressed in μmol/mg dry weight of cells (μmol/mg of cells) [25,26]. *M. luteus* and *E. coli* contain approx. 0.79 μmol and approx. 0.5 μmol of K^+/mg of cells respectively [25]. Concentrations of androctonin were expressed in nmol/mg dry weight of cells (nmol/mg of cells) as a conventional unit for this assay [26].

Oxygen consumption measurements

Oxygen consumption was measured polarographically with a Clarke-type electrode connected to a Gilson oxygraph. Measurements were performed at 37 °C on *M. luteus* (A270) and *E. coli* (D21) cells incubated in the assay medium.

Determination of intracellular and extracellular ATP concentrations

To determine the total (intracellular plus extracellular) concentration of ATP, 20 μl of *M. luteus* (A270) and *E. coli* (D21) were resuspended in the assay medium taken at given times and mixed with 80 μl of Me_2SO. After 30 s at room temperature, the suspensions were diluted with 4.9 ml of cold sterile water. Of this dilution, 0.1 ml was mixed with the luciferin–luciferase reagent (Lumac) and ATP was determined with a Lumac Luminometer. To determine the extracellular ATP concentration, the cell suspensions (0.1 ml) were diluted 1:50 in the assay medium, and ATP was determined with 0.1 ml of this dilution as described above. Experiments were repeated with several culture preparations and gave reproducible results.

Preparation of small unilamellar vesicles (SUV)

SUV were prepared by the sonication of PtdCho/cholesterol (10:1, w/w), PtdEtn/PtdGro (7:3, w/w) or PtdSer/PtdCho (1:1, w/w) [27]. In brief, mixtures of dry lipids were dissolved in chloroform/methanol (2:1, v/v). The solvents were evaporated under a stream of nitrogen; the lipids (7.2 mg/ml) were re-

suspended in buffer by vortex-mixing. The resulting lipid dispersion was sonicated in a bath-type sonicator (G1125SP1 sonicator; Laboratory Supplies Company, Hicksville, NY, U.S.A.) until turbidity had cleared. Vesicles were revealed by electron microscopy (JEOL, Tokyo, Japan) and were shown to be unilamellar with an average diameter of 20–40 nm.

Binding experiments

The interaction of androctonin with vesicles consisting of zwitterionic (PtdCho/cholesterol) or negatively charged phospholipids (PtdSer/PtdCho and PtdEtn/PtdGro) was characterized by measuring changes in the emission intensity of 4-fluoro-7-nitrobenz-2-oxa-1,3-diazole (NBD)-labelled androctonin in titration experiments with SUV. In brief, SUV were added to a fixed amount of peptide (0.1 μM) dissolved in PBS (35 mM phosphate buffer/0.15 M NaCl, pH 7.3) at 24 °C. A glass cuvette (1 cm path length) that contained a final reaction volume of 2 ml was used in all experiments. The fluorescence intensity was measured as a function of the molar ratio of lipid to peptide (four separate experiments) on a Perkin-Elmer LS-5 spectrofluorimeter, with excitation set at 467 nm (10 nm slit) and emission set at 530 nm (5 nm slit). To determine the extent of the lipid's contribution to any given signal, the readings after the addition of lipid vesicles were subtracted as background from the recorded fluorescence intensity. The binding isotherms were analysed as a partition equilibrium by using the following formula [28,29]:

$$X_b = K_P C_f$$

where X_b is defined as the molar ratio of bound peptide (C_b^*) to total lipid, K_P is the partition coefficient and C_f is the equilibrium concentration of the free peptide in solution. For practical purposes it was assumed that the peptides were initially partitioned only over the outer leaflet (60 %) of the SUV. Therefore the partition equation becomes:

$$X_b^* = K_P^* C_f$$

where X_b^* is defined as the molar ratio of bound peptide to 60 % of total lipid and K_P^* is the estimated surface partition constant. The curve resulting from plotting X_b^* against free peptide (C_f) is referred to as the conventional binding isotherm.

Resonance energy transfer measurements

Fluorescence resonance energy transfer was measured by using NBD-labelled peptide as donor and rhodamine-labelled peptide as energy acceptor [30,31]. Fluorescence spectra were obtained at room temperature, with the excitation monochromator set at 460 nm (5 nm slit width) to minimize the excitation of tetramethylrhodamine. Measurements were performed in a glass cuvette (1 cm path length) and a final reaction volume of 2 ml. In a typical experiment, an acceptor (final concentration 0.05–0.3 μM) was added to a donor (final concentration 0.1 μM) in the presence of PtdSer/PtdCho or PtdEtn/PtdGro phospholipid vesicles (300 μM); the degree of the donor's maximum emission quenching and the increase in the acceptor's emission were monitored. The energy transfer was calculated and plotted versus the acceptor/lipid molar ratio. The molar ratios of lipid to peptide in these experiments were kept high (1000:1 to 3000:1) to ensure (1) that most of the peptides were in their membrane-bound state and (2) that a low surface density of donors and acceptors decreased the energy transfer between unassociated peptide monomers. The acceptor peptide was added after the donor peptide had already bound to the membrane to prevent the association of any of the peptides in solution.

Membrane permeability studies

Calcein (molecular mass 623 Da; 60 mM, self-quenching concentration) was entrapped in PtdSer/PtdCho (1:1 w/w) or PtdEtn/PtdGro vesicles in 10 mM Hepes/150 mM NaCl (pH 7.4). The non-encapsulated calcein was removed from the liposome suspension by gel filtration with a Sephadex G-50 (Pharmacia) column connected to a low-pressure liquid chromatography system (Pharmacia). In a typical run, 50 μl of the liposome suspension was injected and eluted in 10 mM Hepes/0.15 M NaCl (pH 7.4). The eluate was monitored by UV absorption (280 nm) and the peak corresponding to vesicles was collected and diluted to 2 ml in the same buffer. Peptides were added to stirred vesicle suspensions (2 ml, 2.4 μM liposomes). Peptide-induced calcein leakage resulted in an increase in fluorescence [32] and was monitored at room temperature (λ_{ex} 485 nm; λ_{em} 515 nm). Complete dye release was obtained after disruption of the vesicles with Triton X-100 [0.1 % (v/v) final concentration]. Under the experimental conditions, in the absence of peptide, the leakage rate was less than 1 % in 5 h. The percentage of fluorescence recovery is defined by comparing dye release with the value obtained after the addition of Triton X-100 (set to 100 %).

Observation of the effects of androctonin on bacteria and vesicles by electron microscopy

Samples containing *E. coli* D21 [10^6 colony-forming units/ml] in Luria–Bertani medium were incubated with the various peptides at their MIC and at one dilution less than the MIC for 1 and 4 h, then centrifuged for 10 min at 300 ***g***. The pellets were resuspended; a drop containing the bacteria was deposited on a carbon-coated grid, which was then negatively stained with 2 % (w/v) phosphotungstic acid, pH 6.8. The grids were examined with a JEOL JEM 100B electron microscope. The effect of androctonin on liposomal suspensions was examined similarly by adding the peptide to SUV composed of PtdSer/PtdCho or PtdEtn/PtdGro at molar ratios of peptide to lipid of 1:40 and 1:80.

Attenuated total reflection–Fourier transform infrared (ATR–FTIR) spectroscopy measurements

Spectra were obtained with a Bruker Equinox 55 FTIR spectrometer equipped with a deuterated triglyceride sulphate detector and coupled with an ATR device. For each spectrum, 200 or 300 scans were collected, with a resolution of 4 cm^{-1}. During data acquisition the spectrometer was continuously purged with dry N_2 to eliminate the spectral contribution of atmospheric water. Samples were prepared as described previously [33]. In brief, a PtdEtn/PtdGro mixture (1 mg; 7:3, w/w) alone or with peptide (50 μg) was deposited on a ZnSe horizontal ATR prism (80 mm × 7 mm). The aperture angle of 45 ° yielded 25 internal reflections. Before sample preparation, the trifluoroacetate counterions, which associated strongly with the peptide, were replaced by chloride ions through several stages of freeze-drying of the peptide in 0.1 M HCl. This allowed the elimination of the strong C=O stretching absorption band near 1673 cm^{-1} [34]. Lipid/peptide mixtures were prepared by dissolving them together in methanol/dichloromethane (1:2, v/v) and drying under a stream of dry nitrogen while moving a Teflon bar back and forth along the ZnSe prism. Polarized spectra were recorded and the respective pure phospholipids in each polarization were subtracted to yield the difference spectra. The background for each spectrum was a clean ZnSe prism. Hydration of the sample was achieved by the introduction of an excess of deuterium oxide

(^2H_2O) into a chamber placed on top the ZnSe prism in the ATR casting and incubation for 2 h before the acquisition of spectra. H/^{2}H exchange was considered to be complete owing to the complete shift of the amide II band. Any contribution of ^2H_2O vapour to the absorbance spectra near the amide I peak region was eliminated by subtraction of the spectra of pure lipids equilibrated with ^2H_2O under the same conditions.

ATR–FTIR data analysis

Before curve fitting, a straight baseline passing through the ordinates at 1700 and 1600 cm^{-1} was subtracted. To resolve overlapping bands, the spectra were processed with PEAKFIT™ (Jandel Scientific, San Rafael, CA, U.S.A.) software. Second-derivative spectra accompanied by 13-data-point Savitsky–Golay smoothing were calculated to identify the positions of the component bands in the spectra. These wavenumbers were used as initial parameters for curve fitting with Gaussian component peaks. Position, bandwidths and amplitudes of the peaks were varied until (1) the resulting bands shifted by no more than 2 cm^{-1} from the initial parameters, (2) all the peaks had reasonable half-widths (less than 20–25 cm^{-1}), and (3) good agreement between the calculated sum of all components and the experimental spectra was achieved ($r^2 > 0.99$). The relative contents of different secondary structure elements were estimated by dividing the areas of individual peaks, assigned to particular secondary structures, by the whole area of the resulting amide I band. The results of four independent experiments were averaged.

Analysis of the polarized ATR–FTIR spectra

The ATR electric fields of incident light were calculated as follows [35]:

$$E_x = \frac{2\cos\theta\sqrt{\sin^2\theta - n_{21}^2}}{\sqrt{(1-n_{21}^2)[(1+n_{21}^2)\sin^2\theta - n_{21}^2]}}$$

$$E_y = \frac{2\cos\theta}{\sqrt{1-n_{21}^2}}$$

$$E_z = \frac{2\cos\theta\cos\theta}{\sqrt{(1-n_{21}^2)[(1+n_{21}^2)\sin^2\theta - n_{21}^2]}}$$

where θ is the angle of a light beam to the prism normal at the point of reflection (45 °), and $n_{21} = n_2/n_1$ [n_1 and n_2 are the refractive indices of ZnSe (taken as 2.4) and the membrane sample (taken as 1.5), respectively]. Under these conditions, E_x, E_y and E_z are 1.09, 1.81 and 2.32 respectively. The electric field components together with the dichroic ratio (defined as the ratio between the absorption of incident light polarized parallel to a membrane plane, A_p, and incident light polarized perpendicularly, A_s) are used to calculate the orientation order parameter, f, by the following formula:

$$R^{ATR} = \frac{A_p}{A_s} = \frac{E_x^2}{E_y^2} + \frac{(E_z^2/E_y^2)[f\cos^2\alpha + (1-f)/3]}{(f\sin^2\alpha)/2 + (1-f)/3}$$

Lipid order parameters were obtained from the symmetrical (approx. 2853 cm^{-1}) and anti-symmetric (approx. 2922 cm^{-1}) lipid stretching mode by using the same equations, setting $\alpha = 90$ ° [35].

RESULTS

Anti-bacterial activities of androctonin, its D-amino acids enantiomer and its fluorescently labelled analogues

Anti-bacterial activities were assessed with the liquid growth inhibition assay on both Gram-positive and Gram-negative bacteria. The results of the inhibitory effect of the peptides are summarized in Table 1. The enantiomer and the fluorescent derivatives retained high anti-bacterial activity. Previous studies revealed that androctonin has no haemolytic activity on human red blood cells when used at concentrations up to 150 μM [21].

Functional studies of androctonin activity against bacterial cells

Measurements of cytoplasmic K^+ efflux, variation of intracellular ATP concentration, and oxygen consumption were conducted to examine the direct effect of androctonin on representative Gram-positive (*M. luteus* A270) and Gram-negative (*E. coli* D21) bacteria. These studies allowed us to examine the correlation

Table 1 Anti-bacterial activities of androctonin and androctonin analogues

The results are expressed as the MIC range, which is the highest concentration tested at which the bacteria are growing and the lowest concentration that causes 100% growth inhibition. Abbreviation: n.d., not determined.

	Antibacterial activity (MIC) (μM)			
Bacterium	Androctonin	All-D-androctonin	NBD-androctonin	Rhodamine-androctonin
E. coli D31	4–8	1–2	1–2	2–4
E. coli D21	32–64	32–64	16–32	16–32
M. luteus	0.5–1	0.5–1	0.25–0.5	0.25–0.5
A. viridans	0.25–0.5	0.5–1	n.d.	n.d.

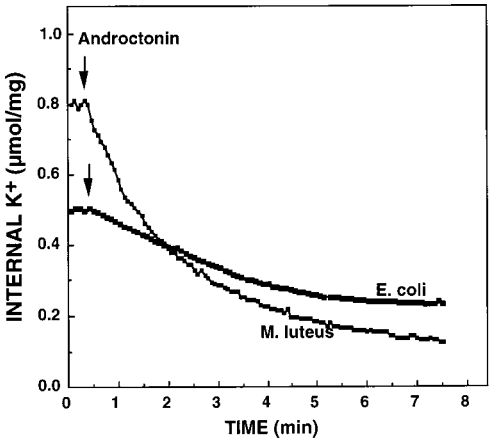

Figure 1 K^+ efflux induced by androctonin

Exponential-phase *M. luteus* and *E. coli* bacterial cells were resuspended in 10 mM Hepes/150 mM NaCl/0.5 mM KCl (pH 7.4) at 37 °C (3 ml of a suspension at a D_{600} of 1). The cells were energized by the addition of 0.2% glucose. Androctonin (130 nmol/mg of cells for *M. luteus*; 200 nmol/mg of cells for *E. coli*) was added after 20 s. K^+ is expressed in μmol/mg dry weight of cells. K^+_{in} was determined as described previously [25].

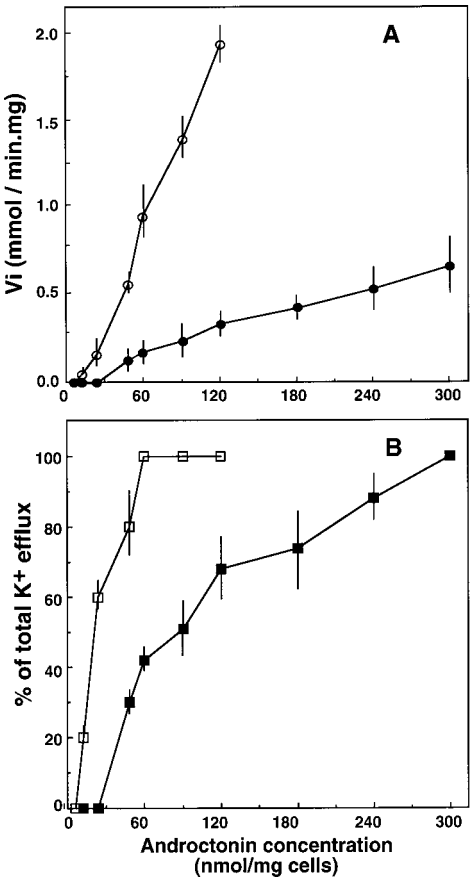

Figure 2 Effect of androctonin concentration on the initial rate (A) and level (B) of K^+ efflux

M. luteus and *E. coli* cells were incubated at 37 °C in 10 mM Hepes/10 mM NaCl (pH 8.6). The assay medium contained 0.2% glucose and 0.5 mM KCl. Symbols: ○, □, *M. luteus*; ●, ■, *E. coli*.

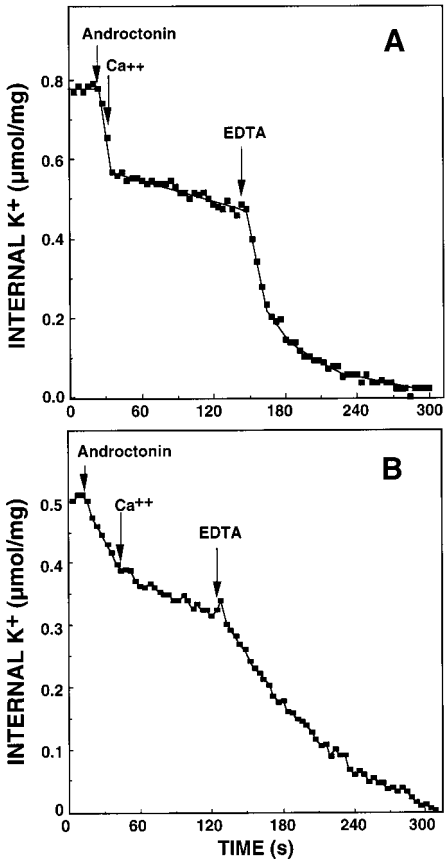

Figure 3 Effect of $CaCl_2$ on androctonin activity

Androctonin (130 nmol/mg of cells for *M. luteus*; 200 nmol/mg of cells for *E. coli*) was added after 20 s to exponentially growing *M. luteus* (**A**) and *E. coli* (**B**) cells. $CaCl_2$ (1 mM) was added after 30–40 s; EDTA (1 mM) was added after 2 min. Experimental conditions were as described in the legend for Figure 1 except that the NaCl was 10 mM and the pH was 8.6.

between the MIC of the peptide, the permeability properties of the cytoplasmic membrane and the bacterial energetic state.

Androctonin induces an efflux of cytoplasmic K^+ from *M. luteus* and *E. coli* cells

The ability of androctonin to induce cytoplasmic K^+ efflux from *M. luteus* and *E. coli* cells was examined under several experimental conditions. In each experiment the ratio between androctonin and the tested bacteria was similar to the MIC found in the inhibition assay (Table 1).

(1) The addition of 40 μM androctonin to the suspension of *M. luteus* cells (130 nmol/mg of cells, equivalent to 0.5 μM in the inhibition assay) incubated at 37 °C in a standard assay medium [10 mM Hepes/150 mM NaCl/0.5 mM KCl (pH 7.4)] resulted in an efflux of cytoplasmic K^+. This efflux started shortly (1–2 s) after the addition of androctonin. After 4 min, the bacteria had lost almost all of their internal K^+. Examples for K^+ efflux in *M. luteus* and *E. coli* are shown in Figure 1. The K^+ efflux was induced by 100 μM androctonin in the suspension of *E. coli* cells (200 nmol/mg of cells, equivalent to 26 μM in the inhibition assay). The lag time (1–2 s) was similar to that for *M. luteus* cells but the initial rate was slower. The slower initial rate might be explained by the fact that androctonin needs to penetrate two cell walls in *E. coli*, a Gram-negative bacterium, compared with one in *M. luteus*, a Gram-positive bacterium.

(2) Decreasing the NaCl concentration from 150 to 10 mM doubled the sensitivity of both *M. luteus* and *E. coli* to androctonin (results not shown).

(3) Decreasing the temperature from 37 to 25 °C did not induce significant variations in the rate of K^+ efflux or in the lag time before efflux, for either bacterium (results not shown).

(4) Increasing the pH of the buffer from 7.4 to 8.8 led to a 5-fold increase in the initial rate and the amount of K^+ lost for both strains (results not shown). The lag time preceding K^+ efflux did not vary with pH (results not shown). All the experiments were repeated five times with different starting colonies of the same bacteria strains; similar curves were obtained. On the basis of these observations further experiments were performed at low ionic strength, at 37 °C and at pH 8.6, which is still in the buffering range of Hepes.

The effect of increasing the concentration of androctonin on the initial rate of K^+ efflux from *M. luteus* and *E. coli* is shown in Figure 2(A), and on the amount of K^+ that was lost in Figure 2(B). The minimal concentrations of androctonin for which an efflux of K^+ was detected were 12 and 50 nmol/mg of cells for *M. luteus* and *E. coli* respectively. These values correspond to an androctonin-to-cell ratio of 2×10^7 for *M. luteus* and 1.5×10^7 for *E. coli*. These thresholds were the same at high (150 mM) and at

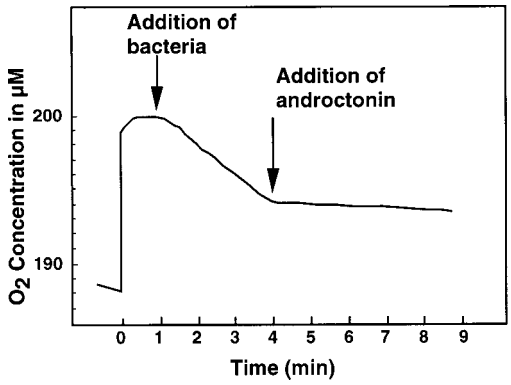

Figure 4 Effect of androctonin on the respiratory activity of *M. luteus* cells

O_2 concentration was measured with a Clarke-type electrode in a buffer [10 mM Hepes/10 mM NaCl (pH 8.6)] maintained at 37 °C. Zero time corresponds to the beginning of recording. Bacteria were added 1 min after O_2 consumption started. The addition of androctonin (92 nmol/mg of cells) after 4 min induced an arrest of O_2 consumption.

low (10 mM) NaCl concentrations (results not shown). The initial rate of K^+ efflux then increased with the concentration of androctonin and showed no saturation up to 120 nmol/mg of cells for *M. luteus* and 300 nmol/mg of cells for *E. coli*. The lag time was always very short and did not vary with the concentration of androctonin for either bacterial strain. The efflux of K^+ was complete only when the concentration of androctonin reached 60 nmol/mg of cells for *M. luteus* and 300 nmol/mg of cells for *E. coli*. These concentrations correspond to the MIC values of androctonin under the same conditions and units (i.e. the range 40–80 nmol/mg of cells for *M. luteus* corresponds to an MIC of 0.5–1 μM; the range 250–500 nmol/mg of cells for *E. coli*. corresponds to an MIC of 32–64 μM).

Effect of bivalent cations on androctonin activity

The addition, after androctonin, of 1 mM Ca^{2+} inhibited the K^+ efflux from *M. luteus* (Figure 3A) and *E. coli* (Figure 3B). This effect was reversed by the addition of 1 mM EDTA. Furthermore, K^+ efflux was prevented if Ca^{2+} was added before androctonin. Again, this effect was reversed by the addition of 1 mM EDTA (results not shown). Experiments were repeated five times with different starting colonies of each bacterial strain; similar curves were obtained.

Effect of androctonin on bacterial respiration measured by oxygen consumption

At 37 °C in the presence of glucose, the O_2 consumption of cells was 30 nmol/min per mg for *M. luteus* [25] and 90 nmol/min per mg for *E. coli* [26]. As shown, for example, in Figure 4 for *M. luteus*, respiration was blocked immediately after the addition of androctonin. This inhibition was observed for pH values ranging from 7.2 to 8.6. The threshold of this inhibitory activity was 12 nmol/mg of cells with *M. luteus* and 50 nmol/mg of cells with *E. coli*; these values are identical with the minimal concentrations of androctonin for which an efflux of K^+ was detected. Complete respiratory inhibition was observed when the MIC of androctonin was reached (60 nmol/mg of cells for *M. luteus*; 300 nmol/mg of cells for *E. coli*). The addition of Ca^{2+} to the buffer abolished the inhibitory effect of androctonin on respiration.

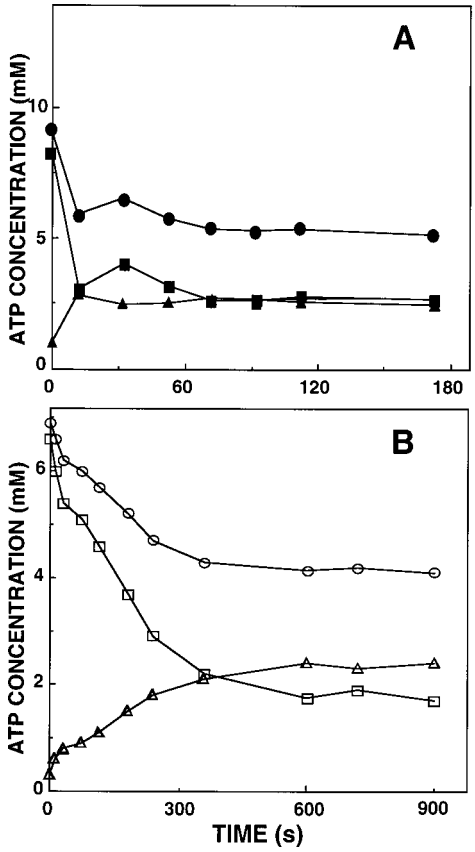

Figure 5 Effect of androctonin on ATP concentration in *M. luteus* (A) and *E. coli* (B) cells

Androctonin (60 nmol/mg of cells for *M. luteus*; 300 nmol/mg of cells for *E. coli*) was added at zero time. Total ATP (●, ○), external ATP (▲, △) and internal ATP (■, □) concentrations were determined at the indicated times.

Effect of androctonin on intracellular ATP concentration

Variation of the intracellular ATP concentration can provide information on bacterial membrane permeation induced by androctonin. On the addition of androctonin at the MIC levels (60 nmol/mg of cells for *M. luteus* and 300 nmol/mg of cells for *E. coli*), there was an immediate and irreversible decrease in the level of ATP. Energized *M. luteus* cells contain 9.3 mM cytoplasmic ATP [25] and *E. coli* 6.9 mM ATP [36]. As shown in Figure 5(A), 45 % of the internal ATP was hydrolysed in *M. luteus*. Concomitantly with this hydrolysis we observed an efflux of 26 % of the ATP, so that at steady state (reached within 3 min) the internal ATP concentration had decreased by more than 70 % of its original value. Under conditions of high ionic strength (150 mM NaCl) the efflux of ATP was similar but the degree of hydrolysis reached 65 %. Similar effects were observed with *E. coli* (Figure 5B).

Effect of androctonin on Gram-negative bacteria

The addition of androctonin to *E. coli* resulted in agglutination of the bacteria even at concentrations at which no efflux occurred (1.5 nmol/mg of cells). This agglutination was reversed by Ca^{2+} ions. The phenomenon was not observed with *M. luteus*.

Interaction of androctonin with phospholipid membranes

The binding of androctonin to vesicles was assessed by using the fluorophore NBD, the fluorescence intensity of which reflects its environment. The fluorescence emission spectrum of NBD-labelled peptide (final concentration 0.1 μM) was monitored in aqueous solution and in the presence of vesicles composed of zwitterionic PtdCho/cholesterol (300 μM) or negatively charged PtdSer/PtdCho or PtdEtn/PtdGro (300 μM each, a phospholipid composition typical of *E. coli*) [37], in PBS at pH 7.1. Changes in fluorescence were recorded as a function of time. After the establishment of a constant fluorescence intensity, the emission spectra were recorded under the same conditions. In these experiments, the molar ratio of lipid to peptide was high (3000:1) so that most of the peptides could be expected to be bound to the vesicles. In buffer, NBD-androctonin exhibited a maximum fluorescence emission at 538 nm (results not shown), which reflects a hydrophilic environment for the NBD moiety [38]. When vesicles were added to the aqueous solutions containing NBD-androctonin, a blue shift in the emission maximum (towards 520 nm) and an increase in the fluorescence of NBD occurred with PtdCho/PtdSer and PtdEtn/PtdGro vesicles but not with PtdCho/cholesterol vesicles. The change in the spectrum of the NBD group reflects its location to a more hydrophobic environment.

The degree of peptide association with lipid vesicles was estimated by peptide titration at a fixed concentration of 0.1 μM and with SUV. The fluorescence values, F, were corrected by subtracting the corresponding blank (buffer with the same amount of vesicles). The increases in the fluorescence intensity, $F-F_0$, where F_0 is the fluorescence intensity in the absence of SUV, were plotted as a function of the molar ratio of lipid to peptide (Figure 6A). The concentration of the peptide was low enough not to disrupt the bilayer structure. No binding could be detected with PtdCho/cholesterol vesicles. The binding curves for PtdSer/PtdCho or PtdEtn/PtdGro vesicles were very similar; the saturation occurred at a molar ratio of lipid to peptide close to 1200.

Binding isotherms were constructed by plotting X_b^* against C_f (Figure 6B). The surface partition coefficients were estimated by extrapolating the initial slopes of the curves to C_f values of zero. The K_p^* of androctonin was $(8.0\pm0.4)\times10^4$ M^{-1} with PtdEtn/PtdGro vesicles and $(4.2\pm0.3)\times10^4$ M^{-1} with PtdSer/PtdCho vesicles (means $\pm$ S.E.M. for four measurements). The shape of the binding isotherm of a peptide can provide information on the organization of the peptide within membranes [39]. The binding isotherm of androctonin with both PtdCho/PtdSer and PtdEtn/PtdGro vesicles was a straight line, indicating a simple adhesion process as opposed to co-operativity in binding. Similar results were obtained with naturally occurring anti-bacterial peptides such as dermaseptins S [40] and cecropins P [41].

Androctonin does not self-associate in the membrane: resonance energy transfer experiments

To evaluate whether androctonin is self-associated in its membrane-bound state, resonance energy transfer measurements were performed, as described previously [40]. For this purpose, NBD-labelled (an energy donor) and carboxytetramethylrhodamine succinimidyl ester (Rho)-labelled (an energy acceptor) androctonin were used. The transfer efficiencies observed were similar to those expected for randomly distributed membrane-bound donors and acceptors [30] with the assumption that R_0 was 51 Å for the NBD/Rho donor/acceptor pair [31] (results not shown). This indicates that androctonin was predominantly in the monomeric form on the surface of the membrane.

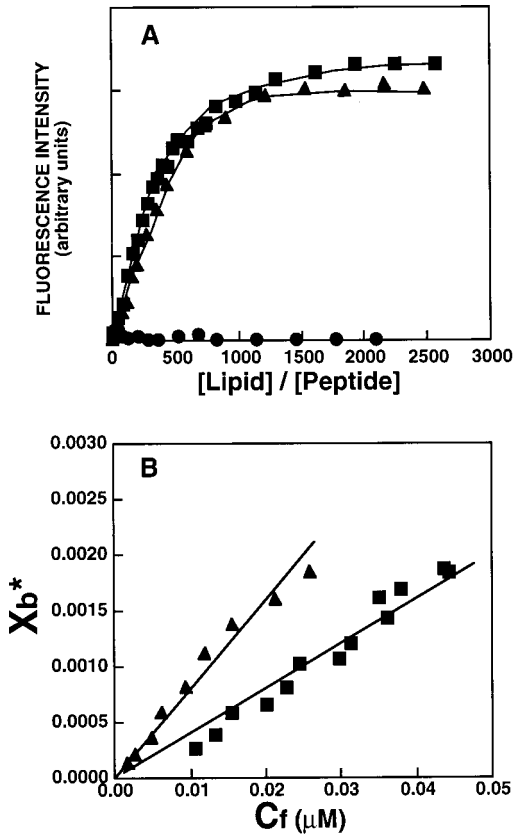

Figure 6 Binding of androctonin to phospholipid membranes

(**A**) Increase in the fluorescence of NBD-androctonin on titration with SUV. NBD-labelled peptide (0.1 μM) in PBS buffer was titrated with SUV composed of PtdSer/PtdCho (■), PtdEtn/PtdGro (▲) or PtdCho/cholesterol (●) at room temperature. The excitation wavelength was 467 nm and emission was monitored at 530 nm. (**B**) Binding isotherms derived from (**A**) by plotting X_b^* (molar ratio of bound peptide per 60% of lipid) against C_f (equilibrium concentration of free peptide in the solution).

Androctonin-induced calcein leakage from vesicles

Androctonin, its D-enantiomer, its fluorescently labelled analogues and dermaseptin S, an amphipathic α-helical anti-microbial peptide that served as a control, were tested for their capacities to evoke calcein release from SUV composed of PtdSer/PtdCho (1:1, w/w) and PtdEtn/PtdGro (7:3, w/w). Increasing amounts of peptides were added to a vesicle suspension at a fixed concentration (2.4 μM). The ability of androctonin and its analogues to permeate the membrane was elucidated by monitoring fluorescence recovery for 15 min; the maximum leakage reached was determined as a function of the molar ratio of peptide to lipid (Figure 7). The D-enantiomer of androctonin and the fluorescently labelled analogues showed the same activity as androctonin; they are therefore not shown. Dermaseptin S induced 100% calcein release from both PtdSer/PtdCho and PtdEtn/PtdGro vesicles with fast kinetics and at a low molar ratio (0.1–0.3) of peptide to lipid. In contrast, androctonin could induce only partial calcein release (25%) from PtdEtn/PtdGro and not at all from PtdSer/PtdCho. The leakage from PtdEtn/PtdGro vesicles was with slow kinetics, at a high molar ratio (1:1) of peptide to lipid. Experiments were repeated three times with an S.D. of 5%.

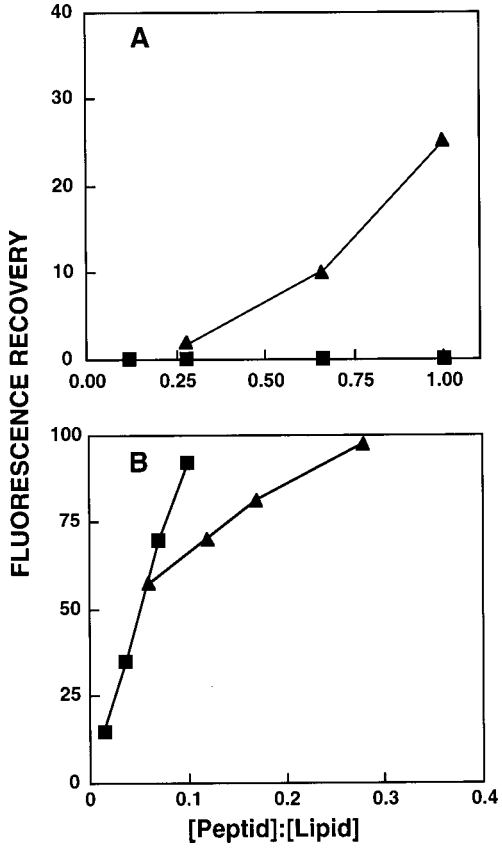

Figure 7 Calcein release induced by androctonin (A) and dermaseptin S (B)

Peptides were added at various concentrations to 2.4 μM PtdSer/PtdCho (■) and PtdEtn/PtdGro (▲) SUV containing entrapped calcein at a self-quenching concentration in 2 ml of buffer [10 mM Hepes/150 mM NaCl (pH 7.4)]. The maximal fluorescence recovery after 15 min was plotted as a function of the molar ratio of peptide to lipid.

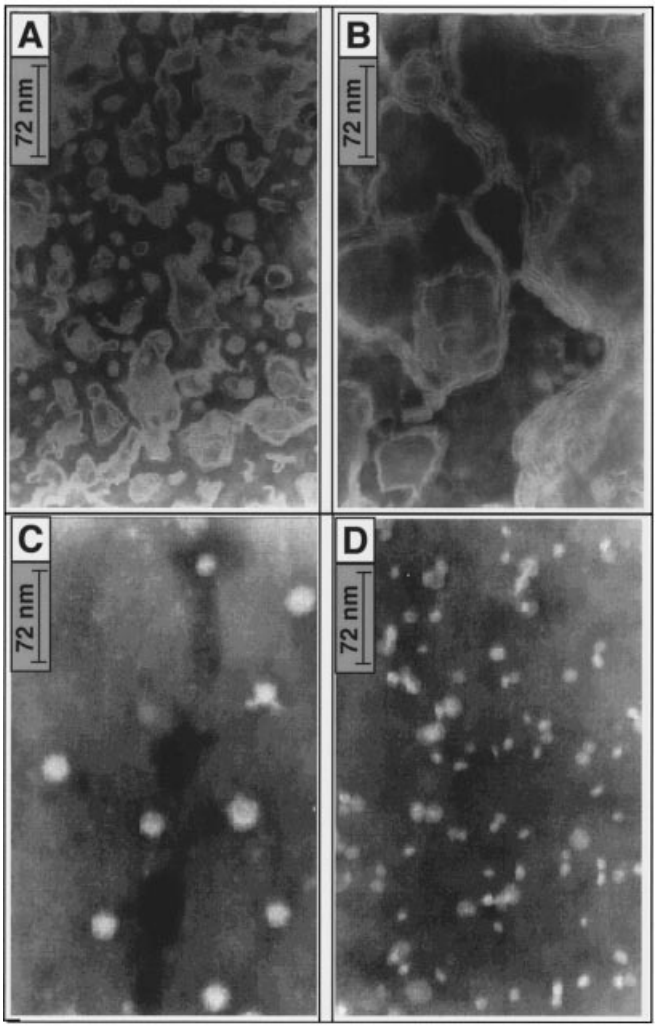

Figure 8 Representative micrographs of SUV composed of PtdEtn/PtdGro or PtdSer/PtdCho in the absence or presence of androctonin at a 1:80 molar ratio of peptide to lipid

(**A**) Untreated PtdEtn/PtdGro; (**B**) PtdEtn/PtdGro treated with androctonin; (**C**) untreated PtdSer/PtdCho; (**D**) PtdSer/PtdCho treated with androctonin.

Electron microscopy study of the effect of androctonin on bacteria and vesicles

The effect of androctonin on the morphology of PtdSer/PtdCho and PtdEtn/PtdGro vesicles, as well as on *E. coli* D21 cells, was studied by transmission electron microscopy. *M. luteus* cells could not be studied in this way because they are lysed to very small pieces. Interestingly, the peptide caused opposite effects on PtdSer/PtdCho and PtdEtn/PtdGro vesicles: whereas androctonin caused a decrease in the size of PtdSer/PtdCho vesicles into small pieces at molar ratios of peptide to lipid of 1:40 and 1:80, it caused an increase of the size of PtdEtn/PtdGro vesicles (Figure 8). The different effects might have arisen from the difference in the composition of the vesicles. PtdEtn/PtdGro is approx. 30% negatively charged with a single charge per PtdGro molecule, whereas PtdSer/PtdCho is 50% charged with a triply charged but net negative (−1) charge. Nevertheless, both effects demonstrated that androctonin was able to interact with, and alter the morphology of, negatively charged membranes. At the MIC, androctonin caused the lysis of large parts of the bacteria (Figure 9C). However, at a concentration lower than the MIC, large blebs were observed on the bacterial wall (Figure 9B). When dermaseptin S was used as a control, small patches were observed (Figure 9D). The blebs might have represented the first step in the lytic process, in which permeabilization of the cytoplasmic membrane occurred and the local accumulation of electron-dense material was released into the periplasmic space.

Determination of the secondary structure of androctonin in PtdEtn/PtdGro phospholipid membranes by FTIR spectroscopy

FTIR spectroscopy was used to determine the secondary structure of androctonin within phospholipid membranes. A spectrum of the amide I region of androctonin bound to PtdEtn/PtdGro (7:3, w/w) multibilayers, a phospholipid composition typical of *E. coli* [37], is shown in Figure 10(A). (PtdSer/PtdCho membranes could not be used for FTIR studies.) Second-derivative analysis revealed that the main amide I maximum (approx. 70%) of the peptide was centred on 1636 cm^{-1}. Minor components were located at 1675 and 1660 cm^{-1}. Assignment of the different secondary structures to the different amide I regions was calculated by using the values taken from Jackson and Mantsch [42]. The amide I region between 1625 and 1640 cm^{-1} was characteristic of a β-sheet structure; the region between 1675 and

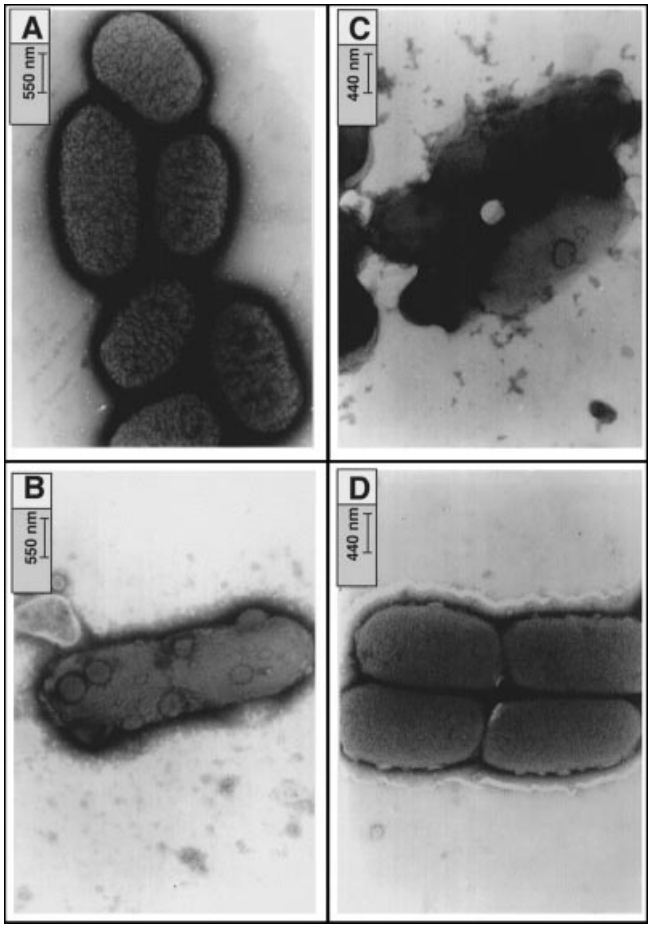

Figure 9 Electron micrographs of negatively stained *E. coli* cells either untreated or treated with androctonin

(**A**) Control; (**B**) treatment of the bacteria with the peptide at a concentration lower than the MIC; (**C**) treatment of the bacteria with the peptide at the MIC; (**D**) similar to (**B**) but with the use of dermaseptin S instead of androctonin.

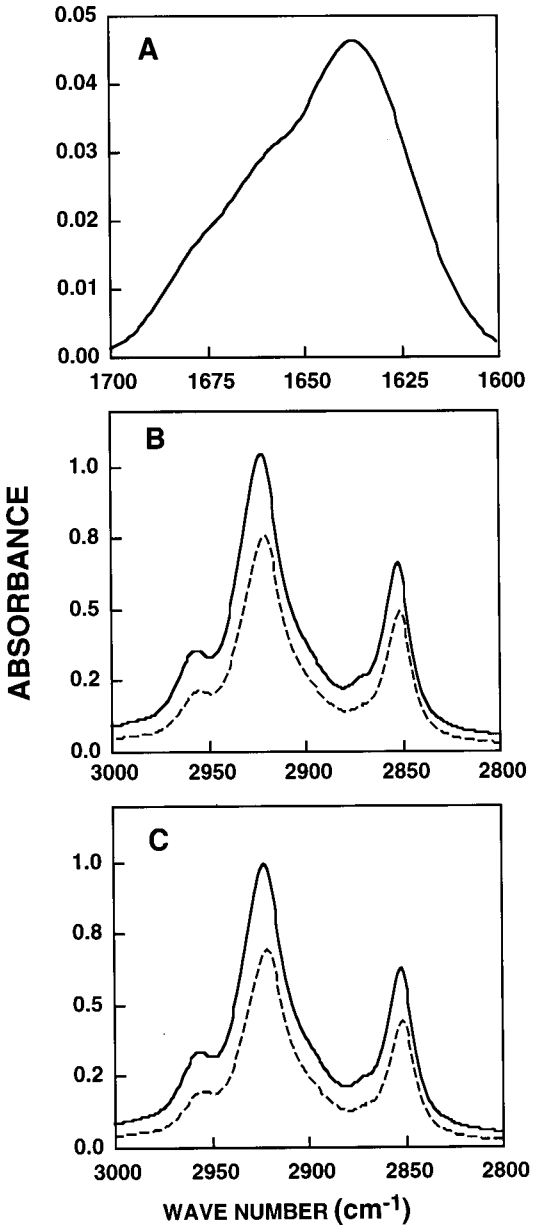

Figure 10 Secondary structure of androctonin in PtdEtn/PtdGro phospholipids and its effect on the acyl chain order

(**A**) FTIR spectrum of the amide I band (1700–1600 cm^{-1}) of androctonin in PtdEtn/PtdGro (7:3, w/w) multibilayer. A 1:80 molar ratio of peptide to lipid was used. The spectrum was analysed by curve-fitting of the amide I band area, assuming Gaussian line shapes for the IR peaks. (**B**, **C**) ATR dichroism spectra of parallel-polarized and perpendicularly polarized ATR–FTIR absorbance spectra between 3000 and 2800 cm^{-1} for the lipid CH_2 symmetrical and anti-symmetric vibration of PtdEtn/PtdGro multibilayers alone (**B**) and incorporated with androctonin (**C**). The top line is for the P component of polarized incident light (an electric vector oscillating parallel to the ZnSe prism or membrane plane) and the bottom line is for the S (perpendicular) component. The molar ratio of peptide to lipid was 1:80.

1695 cm^{-1} was characteristic of an anti-parallel β-sheet structure. The assignment of the band at 1660 cm^{-1} remains uncertain. Previous studies have correlated this band with β-turns, possibly sterically constrained non-hydrogen-bonded amide C=O groups within turns [43]. Deconvolution of the amide I region was performed with PEAKFIT™ and revealed that androctonin adopted $70 \pm 3\%$ β-sheet, $20 \pm 3\%$ anti-parallel β-sheet structures and $10 \pm 3\%$ turns.

Effect of androctonin on order in phospholipid acyl chains

Polarized ATR–FTIR was used to determine the orientation of the lipid membranes and the effect of androctonin on the order in the acyl chains. The symmetrical [$\nu_{sym}(CH_2)$, approx. 2850 cm^{-1}] and the anti-symmetric [$\nu_{antisym}(CH_2)$, approx. 2920 cm^{-1}] vibrations of lipid methylene C–H bonds are perpendicular to the molecular axis of a fully extended hydrocarbon chain. Thus measurements of the dichroism of infrared light absorbance can reveal the order and orientation of the membrane sample relative to the prism surface. The R value based on the stronger $\nu_{antisym}(CH_2)$ was 1.37 ± 0.01. A similar value of R, 1.35, was obtained when $\nu_{sym}(CH_2)$ was used instead (Figure 10B). On the basis of the dichroic ratio of lipid stretching, the corresponding orientation order parameter, f, was calculated to be 0.29 (based on $\nu_{antisym}$) and 0.31 (based on ν_{sym}). The results indicate that the phospholipid membrane is well ordered. The observed antisymmetric and symmetric peaks at approx. 2922 cm^{-1} and approx. 2853 cm^{-1} respectively indicate that the membranes were predominantly in a liquid-crystalline phase [35,44],

as in biological cell membranes. Thus the lipid multibilayer used in our study was well oriented and in a liquid-crystalline phase.

The effect of androctonin on the order in the multibilayer acyl chains can be estimated by comparing the CH_2-stretching dichroic ratio of pure phospholipid multibilayers with that obtained with membrane-bound androctonin. Figure 10(C) shows an example of the ATR dichroism spectra of parallel-polarized and perpendicularly polarized ATR–FTIR absorbance spectra between 2800 and 3000 cm^{-1} of PtdEtn/PtdGro multibilayers incorporated with androctonin. An R value based on the stronger $\nu_{antisym}(CH_2)$ was 1.43 ± 0.02; a similar value of R, 1.41 ± 0.01, was obtained when $\nu_{sym}(CH_2)$ was used instead. The corresponding orientation order parameter, f, was calculated to be 0.26 (based on $\nu_{antisym}$) and 0.27 (based on ν_{sym}). The results indicate that the incorporation of androctonin into the membrane did not significantly change the order of the membrane. These results suggest that androctonin is localized on the surface and does not destabilize the bilayer structure even at high ratios of peptide to lipid.

DISCUSSION

Androctonin, similarly to amphipathic anti-microbial peptides, can inhibit the growth of both Gram-positive and Gram-negative bacteria. The latter have been shown to interact directly with bacterial membranes without a need for specific receptors [45,46]. Their selective activity towards bacteria in comparison with animal cells has been attributed to their preferential binding to negatively charged membranes in comparison with zwitterionic membranes (reviewed in [1–3]). Despite the hydrophilic character of androctonin, the experiments described here suggest strongly that the target of androctonin is also the bacterial membrane. This was demonstrated by several experiments with both bacteria and a phospholipid model system.

(1) The addition of androctonin at the MIC concentration to both Gram-positive (*M. luteus*) and Gram-negative (*E. coli*) bacteria results in an immediate perturbation of the permeability properties of the cytoplasmic membrane and of the bacterial energetic state: cells lose cytoplasmic K^+, their respiration is inhibited and their ATP content is markedly decreased. The effect of androctonin on ATP concentration can be explained both by the efflux of ATP due to permeabilization of the membrane and by the efflux of P_i from the cells due to the hydrolysis of internal ATP [47]. The rapid efflux of these large polar molecules might correspond to the fast disintegration of large zones of the cytoplasmic membrane. The leak of such large and very polar molecules is not observed with peptides that form small pores or channels in the membrane [25].

(2) Electron microscopy revealed that, at the MIC, large parts of the *E. coli* bacteria are lysed. However, at a concentration lower than the MIC, large blebs are observed on the surface of the bacteria (Figure 9). These blebs might be formed owing to the leakage of solutes into the periplasmic space after the permeabilization of the inner membrane of Gram-negative bacteria. The inner pressure could cause the formation of these blebs in the very thin peptidoglycan outer layer of the bacteria. In the next stage, the inflated zone could be perforated and explode, leading to rapid lysis of the cell. This effect seems to be different from that observed with amphipathic anti-microbial peptides such as dermaseptin S (Figure 9D) and others [48,49], in which patches were observed, suggesting more drastic effects on the lipid constituent of the bacterial membrane.

(3) Androctonin binds model phospholipid membranes. However, whereas amphipathic anti-microbial peptides bind strongly to negatively charged membranes and to a smaller extent to zwitterionic ones, androctonin interacts only with negatively charged PtdSer/PtdCho and PtdEtn/PtdGro, and not at all with zwitterionic phospholipids such as PtdCho/cholesterol (Figure 6).

(4) Electron microscopy revealed that androctonin can cause a decrease in the size of negatively charged PtdSer/PtdCho (Figure 8) vesicles without releasing their content, as revealed in the calcein release studies (Figure 7). However, androctonin permeates and increases the size of PtdEtn/PtdGro vesicles (Figures 7 and 8). Androctonin carries a net charge of $+8$; thus electrostatic interactions seem to be important in its initial binding to negatively charged membranes. Once it has bound to the surface of the membrane, it might penetrate into the hydrophobic core of the membrane and disintegrate it in a process similar to that proposed for amphipathic α-helical peptides [50]. However, the hydrophilic character of androctonin does not support its penetration to the hydrophobic core of the membrane. It is more reasonable to assume that its effect results predominantly from a strong interaction with the acidic lipid head groups or the lipid phosphate group, thus disturbing the morphology of the membrane. In agreement with this assumption, the differences in androctonin activity on PtdSer/PtdCho and PtdEtn/PtdGro vesicles might result from the different properties of the negatively charged PtdSer and PtdGro. Whereas PtdGro has a neutral head group and a single negative charge due to the lipid phosphate group, PtdSer has a zwitterionic head group and a net negative charge due to the lipid phosphate group. Thus interaction with the negatively charged head group or the lipid phosphate group might lead to different lipid disruptions. ATR–FTIR studies further support this assumption because androctonin does not significantly perturb the order in the acyl chains (Figure 10). The presence of osmotic pressure can assist in membrane disruption. This might explain the findings that, despite the fact that androctonin has anti-microbial activity similar to that of α-helical anti-microbial peptides, it induces calcein release from PtdEtn/PtdGro vesicles at significantly higher concentrations and slower kinetics than α-helical anti-microbial peptides (Figure 7). Ca^{2+} ions, for example, bind to the lipid head groups of negatively charged vesicles and cause their fusion even though they cannot penetrate into the lipid constituents of the membrane. The relevance of these findings for the biological target membranes of the anti-bacterial peptides is reflected by the fact that the surface of bacteria contains lipopolysaccharide (in Gram-negative bacteria) or polysaccharides (teichoic acids, in Gram-positive bacteria), and that their membranes contain phosphatidylglycerol, all of which are acidic; in contrast, normal mammalian cells (e.g. red blood cells) express predominantly zwitterionic phospholipid PtdCho on their outer leaflet [51,52].

(5) We found that androctonin composed entirely of D-amino acids retained high anti-microbial activity. If molecular interaction with chiral components of the cell membrane were required for anti-bacterial activity, the D-enantiomer would be expected to be inactive. These results are similar to those described for other amphipathic anti-microbial peptides in which the D-enantiomers were as active as the L-enantiomers [45,46], or with the L-enantiomer of HIV-1 fusion peptide [53], the target of which was the phospholipids. These results are in contrast with those obtained with all-D-apidaecin, a proline-rich peptide that totally lost its anti-bacterial activity, suggesting the requirement of recognition between the peptide and a chiral cellular target [54].

The efficiency of the K^+ efflux is higher at basic pH 8.8 than at neutral pH. The pK of the guanidinium group of arginine is 12.5 and that of the amino group of the lysine side chain is 10.8. The

pH shift to 8.8 should have a poor effect on the charge of the peptide but can enhance the negative charge of the bacterial membrane. Consequently the binding of the peptide to the membrane, and the rate and level of K^+ efflux induced by androctonin, are increased. The Ca^{2+}-induced inhibition of K^+ efflux further suggests that the lipid charge has a role in the binding of the peptides to the bacterial membrane. Bivalent cations are known to bind acidic lipids very efficiently [55]. The *M. luteus* membrane contains a high percentage of acidic lipids (diphosphatidylglycerol, phosphatidylglycerol and phosphatidylinositol form 65.5%, 24.5% and 10% of the total lipids respectively) [56]. It is therefore likely that the bivalent cations mask the negative charges of the membrane and can compete with the binding of androctonin to the bilayers. Bivalent cations also increase the ordering of the lipid hydrocarbon chains [55] and can affect the action of androctonin on the membrane.

Androctonin presents some sequence similarities to a family of anti-microbial peptides, the tachyplesins, isolated from the horseshoe crab [20]. These peptides consist of 17 or 18 residues with four cysteine residues engaged in two intramolecular disulphide bridges. In contrast with tachyplesins, which possess a C-terminal arginine α-amide after the C-terminal cysteine residue, androctonin presents a free C-terminal extension of five residues. In addition, the disulphide array (Cys^1–Cys^4 and Cys^2–Cys^3) is identical in androctonin and the tachyplesin family, although the number of residues between the cysteine residues is different. Comparison with the mode of action of this peptide cannot be made, as the latter is still controversial. Two hypotheses have been proposed: (1) tachyplesin acts through a highly efficient mechanism for membrane permeabilization without significantly disrupting the vesicle organization, i.e. anion-selective pore formation followed by translocation [57]; and (2) tachyplesin can act by perturbing membrane organization or by activation–deactivation of membrane surface receptors [58].

In summary, despite its hydrophilic character, androctonin seems to kill bacteria by disrupting the bacterial wall. Its initial binding to bacteria is driven by electrostatic interactions with the negatively charged cell surface, as occurs with amphipathic α-helical peptides. However, in contrast with them its low hydrophobicity prevents it from binding to zwitterionic membranes and therefore makes androctonin more selective for bacteria. The following findings suggest that the membrane disintegration process is achieved via a detergent-like mechanism (a 'carpet-like' model [3,40,41]) rather than the formation of distinct pores or channels. (1) A relatively high androctonin-to-cell ratio (2×10^7) is needed for the lysis of both bacterial types. If all the molecules present in solution were to bind to the bacteria they would almost cover the whole surface of the membrane. (2) No aggregation of androctonin could be detected in solution and in membranes by using rhodamine-labelled androctonin (results not shown). It is thus unlikely that androctonin molecules assemble in the membrane to form pores. (3) ATR–FTIR studies revealed only binding on the surface of the membrane.

Androctonin, which is constitutively present in the haemolymph of scorpion, does not react with scorpion cells. This peptide has no haemolytic properties even at concentration 50-fold the MIC. We have shown that this specificity can be explained by the charge on the bacterial surface. It is well known that the bacterial membrane contains more anionic phospholipids than that of eukaryotic cells. However, to explain this specificity we cannot exclude an effect of stabilization of the membrane by sterols; neither can we exclude the membrane potential, which is higher in bacteria than in animal cells.

This new anti-microbial peptide presents original physicochemical properties: it is a very hydrophilic molecule that differs from most anti-microbial peptides, which present a marked amphipathicity. Androctonin also contains two disulphide bridges that confer a compact structure on this small peptide and make it fairly resistant to the action of proteolytic enzymes. These characteristics are encouraging features for envisaging potential applications in therapeutic use. A better understanding of the molecular mode of action of the anti-bacterial activity of androctonin might therefore lead to the preparation of a more potent anti-bacterial agent.

We thank J.-P. Briand and J.-P. Roussel for peptide assembly, S. Uttenweiler for MS analysis, and Y. Marikovsky for his help with electron microscopy studies. We thank the GDR 790 CNRS for its financial support. This work was supported by the Basic Research Foundation administered by the Israel Academy of Sciences and Humanities, CNRS and the University Louis Pasteur of Strasbourg.

REFERENCES

1 Boman, H. G. (1995) Annu. Rev. Immunol. **13**, 61–92
2 Nicolas, P. and Mor, A. (1995) Annu. Rev. Microbiol. **49**, 277–304
3 Shai, Y. (1995) Trends Biochem. Sci. **20**, 460–464
4 Hoffmann, J. A. and Reichhart, J.-M. (1997) Trends Cell Biol. **7**, 309–316
5 Steiner, H., Hultmark, D., Engstrom, A., Bennich, H. and Boman, H. G. (1981) Nature (London) **292**, 246–248
6 Selsted, M. E., Brown, D. M., DeLange, R. J. and Lehrer, R. I. (1983) J. Biol. Chem. **258**, 14485–14489
7 Zasloff, M. (1987) Proc. Natl. Acad. Sci. U.S.A. **84**, 5449–5453
8 Ganz, T., Selsted, M. E., Szklarek, D., Harwig, S. S., Daher, K., Bainton, D. F. and Lehrer, R. I. (1985) J. Clin. Invest. **76**, 1427–1435
9 Hetru, C., Hoffmann, D. and Bulet, P. (1998) in Molecular Mechanisms of Immune Responses in Insects (Brey, P. T. and Hultmark, D., eds.), pp. 40–66, Chapman and Hall, London
10 Mor, A., Nguyen, V. H., Delfour, A., Migliore, S. D. and Nicolas, P. (1991) Biochemistry **30**, 8824–8830
11 Segrest, J. P., De, L. H., Dohlman, J. G., Brouillette, C. G. and Anantharamaiah, G. M. (1990) Proteins **8**, 103–117
12 Casteels, P., Romagnolo, J., Castle, M., Casteels-Josson, K., Erjument-Bromage, H. and Tempst, P. (1994) J. Biol. Chem. **269**, 26107–26115
13 Bonmatin, J. M., Bonnat, J. L., Gallet, X., Vovelle, F., Ptak, M., Reichhart, J. M., Hoffmann, J. A., Keppi, E., Legrain, M. and Achstetter, T. (1992) J. Biomol. NMR **2**, 235–256
14 Lutke, S. J., He, K., Heller, W. T., Harroun, T. A., Yang, L. and Huang, H. W. (1996) Biochemistry **35**, 13723–13728
15 Bechinger, B. (1997) J. Membr. Biol. **156**, 197–211
16 Shai, Y. (1998) in Molecular Mechanisms of Immune Responses in Insects (Brey, P. T. and Hultmark, D., eds), pp. 111–134, Chapman and Hall, London
17 Lehrer, R. I., Lichtenstein, A. K. and Ganz, T. (1993) Annu. Rev. Immunol. **11**,105–128
18 Selsted, M. E., Tang, Y. Q., Morris, W. L., McGuire, P. A., Novotny, M. S., Smith, W., Henschen, A. H. and Cullor, J. S. (1993) J. Biol. Chem. **268**, 6641–6648
19 Kokryakov, V. N., Harwig, S. S., Panyutich, E. A., Shevchenko, A. A., Aleshina, G. M., Shamova, O. V., Korneva, H. A. and Lehrer, R. I. (1993) FEBS Lett. **327**, 231–236
20 Nakamura, T., Furunaka, H., Miyata, T., Tokunaga, F., Muta, T., Iwanaga, S., Niwa, M., Takao, T. and Shimonishi, Y. (1988) J. Biol. Chem. **263**, 16709–16712
21 Ehret-Sabatier, L., Loew, D., Goyffon, M., Fehlbaum, P., Hoffmann, J. A., Van Dorsselaer, A. and Bulet, P. (1996) J. Biol. Chem. **271**, 29537–29544
22 Neimark, J. and Briand, J.-P. (1993) Peptide Res. **6**, 219–228
23 Hetru, C. and Bulet, P. (1997) in Anti-bacterial Peptide Protocols (Shafer, W. M., ed.), pp. 35–50, Humana Press, Totowa, NJ
24 Casteels, P., Ampe, C., Jacobs, F. and Tempst, P. (1993) J. Biol. Chem. **268**, 7044–7054
25 Cociancich, S., Ghazi, A., Hetru, C., Hoffmann, J. A. and Letellier, L. (1993) J. Biol. Chem. **268**, 19239–19245
26 Boulanger, P. and Letellier, L. (1988) J. Biol. Chem. **263**, 9767–9775
27 Shai, Y., Bach, D. and Yanovsky, A. (1990) J. Biol. Chem. **265**, 20202–20209
28 Rizzo, V., Stankowski, S. and Schwarz, G. (1987) Biochemistry **26**, 2751–2759
29 Schwarz, G., Stankowski, S. and Rizzo, V. (1986) Biochim. Biophys. Acta **861**, 141–151
30 Fung, B. K. and Stryer, L. (1978) Biochemistry **17**, 5241–5248
31 Gazit, E. and Shai, Y. (1993) Biochemistry **32**, 3429–3436
32 Allen, T. M. and Cleland, L. G. (1980) Biochim. Biophys. Acta **597**, 418–426
33 Gazit, E., Miller, I. R., Biggin, P. C., Sansom, M. S. P. and Shai, Y. (1996) J. Mol. Biol. **258**, 860–870
34 Surewicz, W. K., Mantsch, H. H. and Chapman, D. (1993) Biochemistry **32**, 389–394

35 Ishiguro, R., Kimura, N. and Takahashi, S. (1993) Biochemistry **32**, 9792–9797
36 Guihard, G., Bénédetti, H., Besnard, M. and Letellier, L. (1993) J. Biol. Chem. **268**, 17775–17780
37 Shaw, N. (1974) Adv. Appl. Microbiol. **17**, 63–108
38 Rajarathnam, K., Hochman, J., Schindler, M. and Fergusson-Miller, S. (1989) Biochemistry **28**, 3168–3176
39 Schwarz, G., Gerke, H., Rizzo, V. and Stankowski, S. (1987) Biophys. J. **52**, 685–692
40 Pouny, Y., Rapaport, D., Mor, A., Nicolas, P. and Shai, Y. (1992) Biochemistry **31**, 12416–12423
41 Gazit, E., Boman, A., Boman, H. G. and Shai, Y. (1995) Biochemistry **34**, 11479–11488
42 Jackson, M. and Mantsch, H. H. (1995) Crit. Rev. Biochem. Mol. Biol. **30**, 95–120
43 Mantsch, H. H., Perczel, A., Hollosi, M. and Fasman, G. D. (1993) Biopolymers **33**, 201–207
44 Cameron, D. G., Casal, H. L., Gudgin, E. F. and Mantsch, H. H. (1980) Biochim. Biophys. Acta **596**, 463–467
45 Wade, D., Boman, A., Wahlin, B., Drain, C. M., Andreu, D., Boman, H. G. and Merrifield, R. B. (1990) Proc. Natl Acad. Sci. U.S.A. **87**, 4761–4765
46 Bessalle, R., Kapitkovsky, A., Gorea, A., Shalit, I. and Fridkin, M. (1990) FEBS Lett. **274**, 151–155
47 Guihard, G., Bénédetti, H., Besnard, M. and Letellier, L. (1993) J. Biol. Chem. **268**, 17775–17780
48 Alvarez-Bravo, J., Kurata, S. and Natori, S. (1995) J. Biochem. (Tokyo) **117**, 1312–1316
49 Henk, W. G., Todd, W. J., Enright, F. M. and Mitchell, P. J. (1995) Scanning Microsc. **9**, 501–507
50 Oren, Z. and Shai, Y. (1999) Biopolymers **47**, 451–463
51 Verkleij, A. J., Zwaal, R. F., Roelofsen, B., Comfurius, P., Kastelijn, D. and Van Deen, L. L. M. (1973) Biochim. Biophys. Acta **323**, 178–193
52 Op den Kamp, J. A. F. (1979) Annu. Rev. Biochem. **48**, 47–71
53 Pritsker, M., Jones, P., Blumenthal, R. and Shai, Y. (1998) Proc. Natl. Acad. Sci. U.S.A. **95**, 7287–7292
54 Casteels, P. and Tempst, P. (1994) Biochem. Biophys. Res. Commun. **199**, 339–345
55 Düzgünes, N. and Papahadjopoulos, D. (1983) in Membrane Fluidity in Biology, vol. 2 (Aloia, R., ed.), pp. 187–212, Academic Press, New York
56 Barsukov, L. I., Kulikov, V. I., Simakova, I. M., Tikhonova, G. V., Ostrovskii, D. N. and Bergelson, L. D. (1978) Eur. J. Biochem. **90**, 331–336
57 Matsuzaki, K., Yoneyama, S., Fujii, N., Miyajima, R., Yamada, K., Kirino, Y. and Anzai, K. (1997) Biochemistry **36**, 9799–9806
58 Oishi, O., Yamashita, S., Nishimoto, E., Lee, S., Sugihara, G. and Ohno, M. (1997) Biochemistry **36**, 4352–4359

Received 25 August 1999/18 October 1999; accepted 12 November 1999